Chapter 3

Methods for Solar Energy Conversion Efficiency Measurement

3.1 Introduction and Background

As the fields of photoelectrochemical (PEC) energy conversion and solar fuels have grown, a number of metrics have been adopted for evaluating the performance of electrodes and systems. These metrics are often contradictory, irreproducible, or not properly standardized, which prevents researchers from accurately comparing the performance of materials, even within the PEC community itself. We explore herein these different metrics to evaluate their strengths and applicability, as well as to demonstrate the knowledge derived from each approach. We also present a framework for reporting these metrics in an unambiguous and reproducible manner. Additionally, we outline a method to estimate two-electrode system efficiencies from three-electrode potentiostatic measurements, to accelerate the identification of promising system components without requiring the actual construction of a full system. Clarifying these issues will benefit the PEC community by facilitating the consistent reporting of electrode performance metrics, and will allow photoelectrodes and solar fuels systems to be appropriately compared in performance to other solar energy-conversion technologies.

The energy-conversion efficiency is a key metric that facilitates comparison of the performance of various approaches to solar-energy conversion. However, a suite of

disparate methodologies has been proposed and used historically to evaluate the efficiency of systems that produce fuels, either directly or indirectly, with sunlight and/or electrical power as the system inputs. A general expression for the system efficiency is given as the ratio of the total output power (electrical plus chemical) divided by the total input power (electrical plus solar). The solar-to-hydrogen (STH) efficiency follows from this globally applicable system efficiency but is applicable only in the special case for systems in which the only input power is sunlight and the only output power is in the form of hydrogen fuel derived from solar-driven water splitting. Herein, system-level efficiencies, beyond the STH efficiency, as well as component-level figures-of-merit, are defined and discussed to describe the relative energy-conversion performance of key photoactive components of complete systems. These figures-of-merit facilitate the comparison of electrode materials and interfaces without conflating their fundamental properties with the engineering of the cell setup. The resulting information about the components can then be used in conjunction with a graphical circuit analysis formalism to obtain "optimal" system efficiencies that can be compared between various approaches, when the component of concern is used in a reference fuel-producing energy-conversion system. The approach provides a consistent method for comparison of the performance at the system and component levels of various technologies that produce fuels and/or electricity from sunlight.

Many disparate technological approaches are being pursued to convert solar energy into electricity and fuels. For example, photovoltaic (PV) cells, photoelectrochemical (PEC) cells, and solar-thermal systems can directly produce electricity from sunlight. Similarly, fuels can be produced from sunlight either directly

by PEC cells or by solar-driven electricity connected to electrolyzers, either as discrete, stand-alone units or as an integrated system [1, 2]. Fuels can also be generated by thermochemical systems [3-5] or by engineering chemical reactions in biological systems [6]. It is imperative to adopt a consistent approach to report the energy-conversion efficiencies for these various technologies. In all cases, the input power (sunlight, electricity) and output power (electricity, fuels) can be measured by a variety of analytical methods, and the absolute efficiency of any technology can be reported or compared directly to any other.

For solar-fuels generating systems, the solar-to-fuels (STF) efficiency can be directly determined by analysis of the chemical products formed under solar illumination in the absence of an applied bias [7, 8]. The STF efficiency is an important metric for comparing solar-fuels systems to other technologies. However, this metric is reductive by definition, as it does not delineate the sources of loss or sub-optimal performance in a system. A STF metric provides little guidance regarding the potential for improvement because nearly all of the details of performance of the electrodes and of the system design are entangled in this single result. In addition, the STF efficiency is not applicable to systems that require electrical power as a partial input or that produce electrical power as a partial output. Conversely, the electrode *components* of a solar-fuels generating system can be isolated and characterized via electronic and electrochemical methods, and such results can be used to elucidate the catalytic and photovoltaic properties of a component as well as sources of energy-conversion inefficiencies for that component. The translation of these component measurements to STF device performance, however, must be done with care. Furthermore, many electrode component metrics that have

traditionally been denoted and reported as efficiencies for single electrodes are not true efficiencies, because they are not a measurement of the ratio of the total power output to the total power input. Thus, there is a need to improve the evaluation of single prototypical electrodes and to relate their individual performance to their potential in solar-fuels systems.

Herein we first define the system efficiency generally and then more specifically for various technologies that convert sunlight into a combination of electricity and/or chemical fuels. Next we describe related figures-of-merit and discuss their value for the evaluation of single photoactive electrodes within photoelectrochemical STF devices, as well as important considerations towards using such metrics appropriately. To link the properties of photoactive electrodes to the performance of full systems, we present a method of graphical circuit analysis that permits evaluation of the optimal operating point of a hypothetical system composed of electrodes with well-characterized PEC properties. We also discuss how graphical circuit analyses can guide the engineering of an optimally efficient system architecture based on the characteristics of the chosen components. The methods for calculating the optimal system efficiency discussed herein are intended to provide a complementary and general system analysis method relative to evaluating theoretical system efficiencies based on materials properties such as band gaps [9, 10] or relative to measurements of efficiencies in fully realized STF systems [7].

3.2 System Efficiencies

3.2.1 General Treatment

Consider a system that generates output products in the form of chemical fuels and/or electrical power. The total system output power, P_o, is the sum of the output

power contained in the chemical fuel, $P_{f,o}$, and any output power in the form of electricity, $P_{e,o}$. When the incipient output currents, I, due to fuel and electricity production are equal (i.e. the circuit elements are electrically connected in series), this relationship can be expressed as:

$$P_o = P_{f,o} + P_{e,o} = I * \left(E_{f,o} + V_{e,o}\right) \quad (1)$$

where $E_{f,o}$ is the potential difference corresponding to the Gibbs free-energy difference between the two half-reactions of the fuels being produced and $V_{e,o}$ is the output voltage of the electrical power portion of the total system output.

The system inputs may, in general, consist of electrical power, $P_{e,i}$, and/or power from solar illumination, P_s. The total input power, P_i, is therefore:

$$P_i = P_s + P_{e,i} \quad (2)$$

By definition, the efficiency for any process that converts energy from one form to another is the ratio of output power to the input power. The general expression for the *system efficiency* (η) is then simply given by:

$$\eta = \frac{P_{f,o} + P_{e,o}}{P_s + P_{e,i}} \quad (3)$$

The efficiencies of specific technological approaches will be elaborated by examples that are provided in the following sections. For brevity, we do not explicitly treat herein

systems in which the input or output power is composed in part from heat transfer to or from the solar energy-conversion system.

3.2.2 Solar-to-Electricity Systems

For systems that solely produce electricity, such as photovoltaic or regenerative photoelectrochemical cells [11], the maximum-power operating current I_{mp} and voltage V_{mp} are the current and voltage that generate the maximum output power, $P_{max} = I_{mp}V_{mp}$. The efficiency of the photovoltaic or regenerative PEC cell is simply the ratio of the electrical power output to the input power provided by solar illumination. This ratio can be calculated from the general efficiency expression (Equation 3) by setting to zero the terms related to chemical fuel output and electrical power input ($P_{f,o} = 0$ and $P_{e,i} = 0$). Thus, the efficiency of a *photovoltaic or regenerative PEC system* at maximum power, $\eta_{PV,}$ is given by:

$$\eta_{PV} = \frac{P_{e,o}}{P_S} = \frac{I_{mp} * V_{mp}}{P_S} \quad (4)$$

3.2.3 Solar-to-Fuels Systems

For comparing the performance of a solar-fuels generator to a solar-electricity generating system, we adopt herein the Gibbs free energy of the fuel as the standardized measure of the energy content of the fuel [7, 8], where the fuel-forming reactions can be, for example, water splitting, hydrogen halide splitting, CO_2 reduction, etc. For a system that produces only fuel as the output and that uses only solar power as the input, the efficiency can be calculated from Equation 3 by setting to zero the terms related to the electrical power input and output ($P_{e,i} = 0$ and $P_{e,o} = 0$), such that:

$$\eta_{STF} = \frac{P_{f,o}}{P_s} = \frac{A\,[cm^2] * J_{op}\,[A\,cm^{-2}] * E_{f,o}[V] * \varepsilon_{elec}}{P_s\,[W]} \quad (5)$$

where J_{op} is the operating current density, A is the geometric area of the device, and ε_{elec} is the Faradaic efficiency of the fuel production. The solar-to-hydrogen conversion efficiency of a photo-driven water-splitting system is obtained using the difference in formal potentials of the hydrogen-evolution and oxygen-evolution half-reactions ($E_{f,o}$ = 1.23 V) to describe the Gibbs free-energy content of the H_2(g) and O_2(g) formed under standard temperature and pressure conditions. For a photo-driven water-splitting system that produces only H_2(g) and O_2(g) as the outputs, the system efficiency is commonly designated as the *solar-to-hydrogen efficiency*, η_{STH} [7, 12, 13]:

$$\eta_{STH} = \frac{A\,[cm^2] * J_{op}\,[A\,cm^{-2}] * 1.23[V] * \varepsilon_{elec}}{P_s\,[W]} \quad (5')$$

3.2.4 Electricity-to-Fuels Systems

Electrolysis involves the input of electrical power to produce output power as chemical fuel, such as in the form of separated, pure streams of H_2(g) and O_2(g). Electrolyzers operate with no output electrical power ($P_{e,o}$ = 0) and no power generated by illumination (P_s = 0). Assuming that all of the current is derived from Faradaic processes (ε_{elec} = 1), the *efficiency of electrolysis* is:

$$\eta_{\text{electrolyzer}} = \frac{P_{f,o}}{P_{e,i}} = \frac{E_{f,o}}{V_{e,i}} \quad (6)$$

where $V_{e,i}$ is the input voltage required to drive the electrolysis at the operating current density of interest. State-of-the-art electrolyzers require 1.7-1.9 V to effect H_2 production at a current density of 1 A cm^{-2} of projected electrode area, and hence have system efficiencies under such conditions of $\eta_{electrolyzer}$ = 65-75% [14].

3.2.5 Mixed Fuel/Electricity/Solar Input and Output Systems

Efficiencies can also be evaluated from Equation 3 for systems that require electrical and optical energy inputs and/or produce both electrical and chemical energy as outputs. As an example of such a system, an n-Fe_2O_3|1.0 M KOH(aq)|Pt cell can be used as the photoanode in photo-driven water-splitting reactions, and could thus generate a portion of the photovoltage required for electrolysis. However, this system requires an external bias to split water, and therefore η_{STH} is zero by definition as Equation 5 makes no allowance for electrical input power. Nevertheless, the system still provides a net conversion of sunlight in the form of a reduced bias needed to drive the electrolysis reaction relative to the situation with two dark electrodes in the system. Throughout the manuscript, 'dark electrode' refers to an electrode which either has negligible incident illumination incident or is not photoactive. Regardless of the details, the system efficiency can be determined from Equation 3. Because no excess electricity is drawn as output from this cell ($P_{e,o}$ = 0), the expression for the resulting photo-assisted electrolysis system efficiency (η_{PAE}) is:

$$\eta_{PAE} = \frac{P_{f,o}}{P_s + P_{e,i}}. \quad (7)$$

As another example, an n-$SrTiO_3$ photoelectrode operated in aqueous alkaline environment in conjunction with a Pt counter electrode (i.e., an n-$SrTiO_3$|1.0 M KOH(aq)|Pt cell) can perform the full water-splitting reaction without external bias [15]. The photovoltage produced by this system is in excess of that needed for water electrolysis. The η_{STH} value therefore only accounts for the chemical portion of the realizable output power of the system. The excess photovoltage produced by the system could be harnessed as additional power, either as electrical power or as additional chemical output power through the use of engineering methods such as pressurization of the H_2(g) stream (see below). The system efficiency is regardless given by Equation 3 with $P_{e,i} = 0$:

$$\eta = \frac{P_{f,o} + P_{e,o}}{P_s} \tag{8}$$

3.3 System Figures of Merit

Although the system efficiency is the key engineering-based figure-of-merit for fully operational electrochemical solar energy-conversion systems, understanding the electrochemical characteristics of the components of a system is crucial for understanding the results of a system efficiency measurement. Different metrics can be employed to characterize the performance of the photoactive components in systems by varying the components or other inputs of the system. In these cases, a 'system' refers to all of the components of a system that necessarily act in concert to produce harvestable power. This definition of a system can, but does not necessarily, include losses related to electrical generation, transmission, or control as would be considered for large-scale

technical analyses for cross-technology comparisons. These measurements are often taken on systems employing two electrodes in an electrochemical cell.

One quantity that has been used to describe the performance of photoactive electrodes is the *applied-bias photon-to-current* metric (often called an efficiency, and thus often abbreviated ABPE or ABCE, abbreviated here as ABPC) [16, 17]. As given in Equation 9, this quantity is the difference of the power output in chemical fuel and any added electrical input power, divided by the solar power input [15, 18]:

$$\phi_{ABPC} = I_{mp} * \frac{(E_{f,o} - V_{ext,mp})}{P_s} \quad (9)$$

Here I_{mp} is the current at the maximum power point, $E_{f,o}$ is the potential difference corresponding to the Gibbs free energy of the fuel being produced, and $V_{ext,mp}$ is the applied voltage at the maximum power point between the working photoactive electrode and a standard dark counter electrode.

Φ_{ABPC} is the IUPAC-suggested definition of the solar-conversion efficiency of a cell that has a dark electrode and a semiconductor-based photoactive electrode [18]. In general, however, Φ_{ABPC} is not a measurement of a system efficiency, because Φ_{ABPC} is not a ratio of the total power output divided by the total power input to the system. Rather, Φ_{ABPC} measures the net chemical output power (rate of production of free energy of products less the input electrical power) of a system in units of incident solar power. The Φ_{ABPC} figure-of-merit represents the fraction of the energy stored in the chemical products that can be assigned to the photovoltage provided by the input solar illumination. The value of Φ_{ABPC} can be negative, meaning that the electrical energy

input even under illumination is in excess of the free energy stored in the products. For systems that perform fuel-forming reactions without an applied bias (V_{ext}), the expression for Φ_{ABPC} reduces to the analytical form of η_{STH} (Equation 5) if no electrical power is output by the system.

Another metric commonly used to evaluate the effects of input solar illumination is the system-level *power-saved* metric. This metric is quantified by determining the external voltage needed to achieve a current, *I*, for a system with a photoactive working electrode and a given counter electrode, compared to the voltage needed to achieve that same current in a related system but comprising instead a dark working electrode and the same counter electrode:

$$P_{saved}(I) = I * \left(V_{dark,ext}(I) - V_{light,ext}(I)\right) = I * V_{saved}(I) \qquad (10)$$

where $V_{dark,ext}(I)$ and $V_{light,ext}(I)$ are the measured external bias values needed to drive the reaction at current *I* in the dark and light, respectively, and $V_{saved}(I)$ is the difference between $V_{dark,ext}(I)$ and $V_{light,ext}(I)$. Throughout this manuscript, '*' is used to imply multiplication, and conversely a variable followed immediately by another variable in parentheses indicates that the former variable is a function of the latter. The ratio of the saved power to the input solar power is a commonly reported metric based on the power-saved measurement [19], and thus the *ratiometric power saved* is given as:

$$\Phi_{saved} = \frac{I*V_{saved}}{P_S}. \qquad (11)$$

The power-saved metric is further discussed in three-electrode measurements (see section IV.A), because for a given current, the measured quantity is identical for two- and three-electrode configurations.

3.4 Three-Electrode Measurements

Three-electrode electrochemical current density vs. potential (*J-E)* measurements provide a direct evaluation of the properties of an electrode under the relevant solution and illumination conditions, and can be replicated readily by other researchers. This provides a distinct advantage over the less easily replicated two-electrode system measurements discussed above. This fundamental evaluation of electrode performance provides a basis to compare the relative metrics for different electrodes. Furthermore, three-electrode measurements allow identification of the optimal performance achievable in a system that would use the given components, without having to explicitly consider or develop the design, engineering, or operational details of the full system.

In three-electrode voltammetric measurements, a potentiostat is used to control the potential difference between a working electrode and a reference electrode, while the current is measured between the working electrode and a counter electrode, with negligible current passed between the working and reference electrodes. The *J-E* behavior can therefore be determined independently of any overpotentials, mass-transport restrictions of redox species, and potential drops associated with the counter electrode and the counter electrode-electrolyte interface, or of the solution ohmic losses between the working and counter electrodes. Kinetic overpotential and mass transport losses may be considered inherent to an electrode under the relevant conditions, but potentiostatic

measurements should always be appropriately corrected for any uncompensated solution resistance, as this quantity is not a fundamental characteristic of an electrode/electrolyte interface.

For photoactive electrode components, the *J-E* behavior can yield the *open-circuit potential*, E_{oc}, the current at the Nernstian potential ($E(A/A^-)$) for the half-reaction of interest, $I(E(A/A^-))$ (or $J(E(A/A^-))$, the current density), and the photogenerated current, I_{ph} [20], determined by finding the difference between the current under illumination and the dark current, prior to the observation of breakdown phenomena and under conditions that are not mass-transport limited. When I_{ph} is potential-dependent (e.g. due to photogenerated carrier collection being dependent on drift in the depletion region) I_{ph} should be measured separately at each potential of interest.

3.4.1 Power-Saved Metric

In a three-electrode system, the power saved [16, 21, 22] at any current, I, is given by the product of the current I and the difference between the potential required to drive a half-reaction at a selected working electrode at this current in the dark, $E_{dark}(I)$ and the potential required to drive the same half-reaction at a photoactive electrode in the light, $E_{light}(I)$:

$$P_{saved}(I) = I * \left(E_{dark}(I) - E_{light}(I)\right) = I * V_{saved}(I) \quad (12)$$

The *ratiometric power saved* is still given by P_{saved} divided by the input solar power, P_s:

$$\phi_{saved} = \frac{I*V_{saved}(I)}{P_s}. \quad (13)$$

Because the power-saved measurements are, by definition, differences in performance between the photoactive electrode and a selected dark electrode, all of the cell and system-based losses in a two-electrode system and in a three-electrode cell should cancel out in the calculated power saved difference measurements. Therefore, a power-saved measurement extracted from two three-electrode measurements (Equation 10) is identical to a power-saved measurement obtained from two two-electrode measurements (Equation 12), at a given value of *I*.

Figure 3.1 illustrates the different methods by which three-electrode power-saved measurements can be used to characterize the photoactive electrode performance.

3.4.4.1 Power-Saved Measurements Relative to an Ideally Nonpolarizable Dark Electrode

If the photoactive electrode is compared to an ideally non-polarizable dark electrode for that same half-reaction (Figure 3.1a), the potential difference at a given current is then:

$$E_{dark}(I) - E_{light}(I) = E(A/A^-) - V_{PV}(I) + V_{cat}(I) + V_{mt}(I) + V_{sol}(I)) \quad (14)$$

where $V_{PV}(I)$ is the ideal *I-V* characteristic of the photoactive electrode, $V_{cat}(I)$ is the potential loss due to the catalytic overpotential, $V_{mt}(I)$ is the potential loss due to mass transport, and $V_{sol}(I)$ is the potential loss due to ohmic solution resistance. $E_{light}(I)$ and $E_{dark}(I)$ are the voltammetric *I-E* measurements of the working photoactive electrode of

interest and the dark electrode of comparison, respectively. Equation 14 contains no potential drops for the dark electrode because an ideally non-polarizable electrode remains at a fixed electrochemical potential regardless of the current flowing through the interface. The potential of the electrodes is controlled by an external control source, such as a potentiostat.

Multiplying by the current and dividing by the input solar power yields:

$$\phi_{saved,ideal} = \frac{I*[V_{PV}(I)-(V_{cat}(I)+V_{mt}(I)+V_{sol}(I))]}{P_S} \quad (15)$$

In the example from Figure 3.1a, the ratiometric power-saved at the maximum power point is $\phi_{saved,ideal}$ = 0.008 A x (1.23V-0.71 V) / P_s = 4.2% for P_s = 0.1 W cm^{-2}. The value of $\phi_{saved,ideal}$ has often been designated as an efficiency, sometimes called the thermodynamic energy conversion efficiency and other times, if corrected for concentration overpotentials and uncompensated resistance losses, called the intrinsic photoactive electrode efficiency. However, neither quantity as calculated is an actual system efficiency, because the calculated quantities do not represent a ratio between the total power output by, and total power input into, a full system. The value of $\phi_{saved,ideal}$ can, however, be used to obtain a specific type of system efficiency, provided that the working photoactive electrode is used in conjunction with an ideally nonpolarizable counterelectrode in an ideal electrochemical cell, as described in section VI.A below.

3.4.4.2 Power-Saved Measurements Relative to a State-of-the-Art Dark Electrode

The photoactive electrode power saved can also be calculated with respect to a state-of-the-art dark electrode for the half-reaction of interest (Figure 3.1b, $\phi_{saved,SOA}$). The potential difference at a given current is then:

$$E_{dark,SOA}(I) - E_{light}(I) = \left(V_{cat,dark}(I) - V_{cat,light}(I)\right) + \left(V_{mt,dark}(I) - V_{mt,light}(I)\right) + V_{PV}(I) \quad (16)$$

where $V_{cat,dark}(I)$ and $V_{mt,dark}(I)$ are the potential losses due to catalysis and mass transport, respectively, at the state-of-the-art dark electrode, $V_{cat,light}(I)$ and $V_{mt,light}(I)$ are the potential losses due to catalysis and mass transport, respectively, at the photoactive electrode, and $E_{dark,SOA}(I)$ is the voltammetric *I-E* measurement of the state-of-the-art dark electrode of comparison.

As seen in Equation (16), comparison of a photoactive electrode to a state-of-the-art dark electrode takes into account any differences in the catalytic activities of the electrodes, any differences in mass transport to the electrode surfaces, and accounts for the photovoltage generated by the photoactive electrode. In the example from Figure 3.1b, the measured ratiometric power-saved at the maximum power point is $\phi_{saved,SOA}$ = 0.008 A x (1.23 V+0.10 V-0.71 V) / P_s = 5.0%.

3.4.4.3 Power-Saved Measurements Relative to a Dark Degenerately Doped Catalytic Anode to Isolate the Photovoltage-Current Performance of a Photoactive Electrode

The photoeffects produced by an illuminated photoactive electrode can be isolated from catalytic losses or from cell resistance or concentration overpotential losses by use of a non-photoactive version of the illuminated electrode of interest (*e.g.* a p^+-Si dark anode compared to an n-Si illuminated photoanode) as the dark electrode for a three-electrode power-saved measurement. In this case (Figure 3.1c), in an otherwise identical 3-electrode electrochemical cell, the power saved ($\phi_{saved,NPA,C}$) (NPA,C = non-photoactive, identical catalyst) calculated by subtraction of E_{light}, the potential applied to the photoactive electrode, from the value of E_{dark} exhibited by a non-photoactive dark electrode, both at a given current I, is given by:

$$E_{dark}(I) - E_{light}(I) =$$
$$(E(A/A^-) - V_{PV}(I) + V_{cat}(I) + V_{mt}(I) + V_{sol}(I)) - (E(A/A^-) + V_{cat}(I) + V_{mt}(I) + V_{sol}(I))$$
$$= V_{PV}(I) \quad (17)$$

where the photopotentials in Equation 17 have been broken down into the various components that represent the photovoltaic component, V_{PV}, the overpotential due to electrocatalytic losses, V_{cat}, the overpotential due to mass transport losses/concentration overpotentials, V_{mt}, and the voltage losses due to uncompensated solution resistance, V_{sol}. $E(A/A^-)$ is the Nernstian potential of the half-reaction being performed at the working electrode. The value of V_{saved} produced by such a calculation isolates the photovoltage

$V_{PV}(I)$ generated by the photoactive electrode in the limit where the catalytic/mass transport behavior of the photoactive working electrode and of the dark working electrode are the same and therefore cancel in the subtraction of E_{dark} from E_{light}. In the example from Figure 3.1c, the measured ratiometric power-saved at the maximum power point is $\phi_{saved,NPA,C}$ = 0.008 A x (1.23V+0.2V-0.71V) / P_s = $\phi_{saved,NPA,C}$ = 5.8%.

The *photovoltaic characteristics*, $V_{PV}(I)$, of a photoactive electrode can be described by the diode equation:

$$V_{PV}(I) = \frac{nkT}{q} * \ln\left(\frac{|I_{ph}|-I}{|I_0|} + 1\right) \quad (18)$$

where n is the ideality factor of the photodiode, k is Boltzmann's constant, T is the absolute temperature, q is the unsigned elementary charge on an electron, I_{ph} is the light-induced current of the photodiode, and I_0 is the reverse-saturation current of the photodiode. Extraction of the $V_{PV}(I)$ behavior allows analysis that the observed *J-E* performance of the photoactive electrode could equivalently instead be obtained through the use of an external PV cell connected electrically in series with an electrocatalytic dark electrode, with the PV cell required to exhibit specific values of its V_{oc}, short-circuit current, fill factor, and thus an energy-conversion efficiency (as defined by Equation 4).

3.4.4.4 Power-Saved Measurements Relative to Other Types of Working Electrodes

In general, other choices of working electrodes for use in power-saved measurements will yield a convolution of effects due to the photovoltaic properties and catalytic properties, and the photoactive electrode and dark electrodes used in the comparison. For instance, if a degenerately doped photoanode is used as the dark electrode for the power saved measurement[19 19], the resulting value will also include any overpotentials associated with rectifying behavior of the semiconductor/liquid junction at reverse bias, and possibly ohmic resistance losses between the back contact and the reverse biased semiconductor electrode. The "ideal" degenerately doped dark anode would show none of these losses and thus would ultimately produce an ideally nonpolarizable working electrode. Other degrees of rectification would produce a convolution of the polarization behavior of the dark anode with the photoanode characteristics, making it difficult to extract either pure values for $V_{PV}(I)$, $V_{cat}(I)$, $V_{mt}(I)$, or $V_{sol}(I)$ from the difference between the *J-E* behavior of the photoactive electrode and the *J-E* behavior of the dark anode. Ideally behaving, non-degenerately doped semiconductor electrodes will exhibit negligible dark current well into reverse bias [20, 23]. In such systems, Equation 18 applies over a wide range of voltages, and hence $J = J_o$ even for very large reverse biases. Therefore, for such systems, the use of the dark *J-E* characteristic as a reference for power-saved measurements, relative to the *J-E* characteristics for that same photoactive electrode under illumination, will produce misleadingly large power-saved values. For example, an n-Si-based photoanode exhibits negligible dark current even at very large reverse bias potentials [24, 25]. The comparison

between the dark anodic current and illuminated anodic photocurrent on the same electrode would in this case result in 'photovoltages' derived from the power-saved calculation that were misleadingly large, and would yield values in excess of the band-gap energy of Si.. Similarly, the use of a dark anode with a very high overpotential for the reaction would inherently include a very large value for $V_{cat,dark}$, which would not provide a consistent basis for calculation of solely either $V_{PV}(I)$, $V_{cat}(I)$, $V_{mt}(I)$, or $V_{sol}(I)$ from a power-saved measurement.

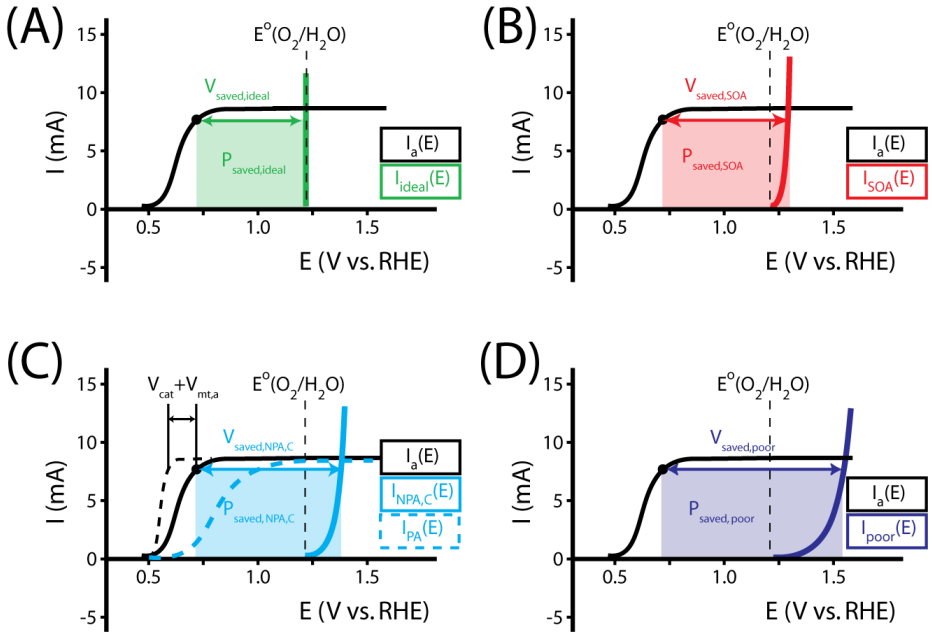

Figure 3.1. Examples demonstrating the effect of the chosen comparison dark electrode on the power-saved figure-of-merit in three-electrode *J-E* measurements. In each example, the same schematic voltammetric *I-E* characteristic (maximum power point designated by a black dot; V_{mp} = 0.71 V vs. RHE, I_{mp} = 8 mA, electrode area = 1cm^2) for the photoanode of interest is compared to a chosen dark electrode performing the same anodic reaction. (A) The power-saved compared to an ideally non-polarizable dark electrode. The measured ratiometric power-saved is $\phi_{saved,ideal}$ = 4.2% (for P_s = 0.1 W cm^{-2}). (B) The power-saved compared to the state-of-the-art dark anode for the water oxidation reaction (see Table 3.1). In this example, the dark electrode exhibits an overpotential of 100 mV at I = 8 mA, increasing the measured ratiometric power-saved value to $\phi_{saved,SOA}$ = 5.0%. (C) The power-saved by the photoanode compared to an identically engineered (semiconductor substrate, structure and mass loading of electrocatalyst, surface, etc.), non-photoactive, degenerately doped electrode (solid blue line). For the example that the catalyst and mass-transport overpotentials are 200 mV for this electrode configuration, and the ratiometric power-saved value is $\phi_{saved,NPA,C}$ = 5.8%. The intrinsic photovoltaic properties of the semiconductor $V_{PV}(I) = E_{dark,NPA,C}(I)$-$E_{light}(I)$ (dashed black line). The catalyst/mass transport effects can be observed using a photoactive electrode prepared from the photoactive substrate without added electrocatalyst ($E_{light,PA}(I)$) (dashed blue line, PA = Photoactive). (D) The power-saved for the photoanode compared to a dark electrode with a non-optimal catalytic overpotential for water oxidation. An arbitrarily poor dark electrode can be chosen for comparison, which increases the ratiometric power-saved metric ($\phi_{saved,poor}$ = 6.6% for the example dark electrode with overpotential of 300 mV at 8 mA) without any actual improvement in the photoactive electrode characteristics.

3.5 Predicting System Efficiencies from Three-Electrode Component Measurements

To determine how a particular component will affect the overall efficiency of a system, the most rigorous approach is to physically construct a full system that includes the component in question. However, this method introduces unreasonable barriers to component-level research because only those research groups capable of building and accurately testing full photoelectrochemical systems would then be able to participate in component-level development. Additionally, a lack of standardization in device and system designs can lead to different conclusions between different laboratories regarding the contribution of the same component to the performance of the same device.

An alternative approach is to hypothetically integrate the components into a theoretical, optimized system in which the resistive losses associated with the solution, membrane, and series resistances are negligible. This process allows estimation of an optimal system efficiency for a given photoactive electrode, and the resulting optimal system efficiency value can be compared directly to efficiencies of other full systems. While this optimal system efficiency will always be greater than the measured efficiency for an actual, constructed device, calculation of the optimal system efficiency is nevertheless a valuable evaluation of how individual components will contribute to the system efficiency in an optimized device configuration. Below, we describe a method to determine the optimal system efficiency from half-cell measurements for three different photoelectrochemical systems: 1) an ideal regenerative photoelectrochemical cell, 2) a photoassisted electrolysis device, and 3) a dual-photoactive electrode photosynthetic cell.

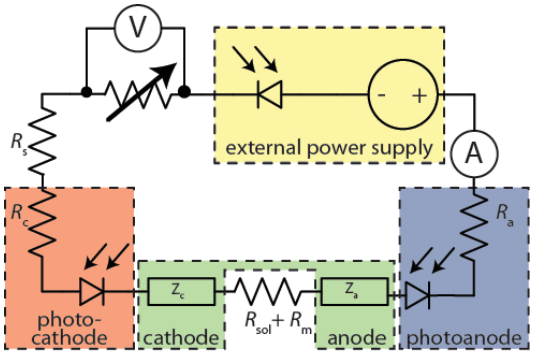

Figure 3.2. An equivalent circuit for a full two-terminal electrochemical system that allows for the inputs of electrical power as well as solar power at various stages. The resistance and impedance characteristics of each electrode can be determined by electrochemical measurements. For a graphical circuit analysis, the relevant electrochemical behavior can be determined from IR-corrected, three electrode *J-E* measurements.

3.5.1 Graphical Circuit Analysis For Identifying System Efficiencies From Three-Electrode Measurements

Figure 3.2 shows an equivalent circuit diagram for a two-electrode system. The photoelectrochemical characteristics of a photoanode/anode and of a photocathode/cathode components are determined by their representative individual *IR*-corrected *J-E* measurements. To perform the graphical circuit analysis, the cathodic *J-E* characteristic (referenced to the Nernstian potential of the reaction at the cathode) is reflected across the x-axis and translated by V_{app}, thus crossing the anodic *J-E* characteristic (referenced to the Nernstian potential of the reaction at the anode). The *operating current* I_{op} can be identified by the intersection point at which the current has

the same absolute value through the anode and through the cathode. This constraint can be understood as a requirement of Kirchoff's current law that the current through each electrode must be the same. The value of the efficiency at zero applied bias and the applied bias that results in the maximum efficiency can then both be readily computed. This method is analogous to typical load-line analyses of photovoltaic cells and resistive loads. The *J-E* behavior of an electrode is obviously dependent on the composition of the solution including the concentration of both electrolyte and gaseous species, the incident illumination on the electrode, and the temperature of the cell, among other factors. Whenever possible, the three-electrode measurements used in the graphical circuit analysis to produce predicted optimal system efficiencies should therefore be obtained under the same conditions that the electrode will experience during steady-state operation in the relevant two-electrode device. If both of the three-electrode measurements are not obtained under the same solution conditions (e.g. different counter ions, different pH, etc.) except for any separated products that may appear at one electrode but not the other (e.g. O_2 gas at an anode and H_2 gas at a cathode), correction for any junction potential that would form or equilibration of electrolyte that would take place in the two-electrode device is necessary.

3.5.1.1 Ideal Regenerative Cell Efficiency

Figure 3.3 shows the graphical circuit analysis for an ideally nonpolarizable counter electrode performing the same chemical half-reaction (but in the opposite direction chemically) as is being performed by the working electrode. This system constitutes a regenerative photoelectrochemical cell, in which input solar power produces

only electrical power as the output, with no net chemical change in the components of the cell itself.

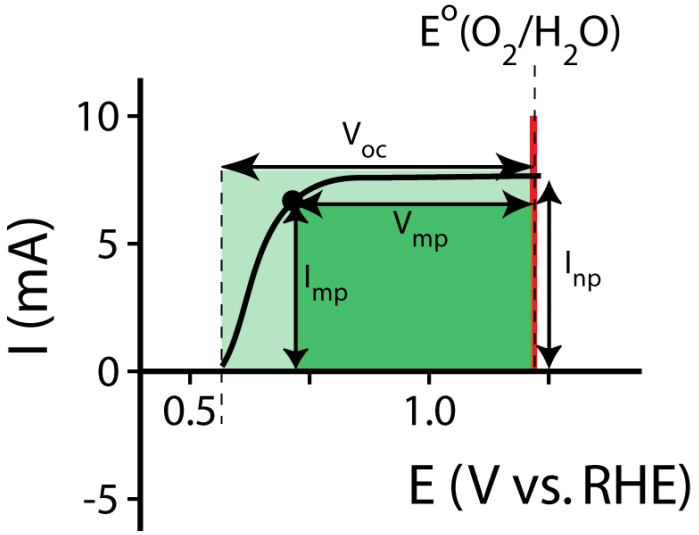

Figure 3.3. The calculation of the intrinsic regenerative cell efficiency, η_{IRC}, of an example photoanode in a configuration where water is being oxidized at the photoanode (black), and oxygen is being reduced at an ideally polarizable counter electrode (red). The system efficiency η_{IRC} can be calculated from the output power at the maximum power point, indicated by the black dot on the voltammagram of the photoanode.

These conditions are fully analogous to those of a solid-state photovoltaic cell, and therefore the same equation is used as the relationship that describes the efficiency of a PV device:

$$\eta_{IRC} = \frac{V_{mp} * I_{mp}}{P_s} = \frac{I(E(A/A^-)) * V_{oc} * ff}{P_s} \qquad (19)$$

where η_{IRC} is the *ideal regenerative cell efficiency*. The values of V_{oc} and $I(E(A/A^-))$ in Equation 19 are both referenced to the equilibrium potential of the half-reaction being

performed at the photoactive electrode. The fill factor (*ff*) is the ratio of the power out at the maximum power point (V_{mp} x I_{mp}) to the product V_{oc} x $I(E(A/A^-))$. The fill factor is a common metric used to quantify the fraction of the theoretical maximum power that is achieved from a photovoltaic, and is determined from a *I-E* measurement corrected for the solution potential drop (V_{sol}) and also possibly for any correctable (see below) mass-transport-derived voltage losses (V_{mt}). The value of η_{IRC} is a true system efficiency that, by construction, is numerically equal to $\phi_{saved,ideal}$ (Equation (19)) calculated from 3-electrode measurements as described in section IV.4.

The η_{IRC} efficiency shares similarities with the two-electrode Φ_{ABPC} metric. As noted earlier, the voltage used to obtain a value for η_{IRC} is exactly the load voltage. Because η_{IRC} is designed to describe the behavior of a regenerative cell, the load is adjustable. However, the load is not adjustable for the fuel-forming systems that Φ_{ABPC} is used to describe. For fuel-forming reactions, in general, the free energy of formation of the chemical fuel is the load in an electrochemical solar-driven water-splitting cell. Thus, for water splitting, a value of 1.23 V is used for the load. This value appears in Equation 9, and the $\boldsymbol{\Phi}_{\mathbf{ABPC}}$ metric and η_{IRC} would thus have mutually identical numerical values for a fuel-forming system in which $V_{ext} = 0$ and for which the counter electrode was ideally non-polarizable.

3.5.1.2 Optimal System Efficiencies

An *optimal system efficiency*, η_{opt}, can be defined for a system that consists of the specified working photoactive electrode and an optimized, state-of-the-art counter electrode that has explicitly stated component-level performance characteristics, while assuming that all other voltage losses are negligible. The merit of this approach is that it produces a standardized, self-consistent set of calculated solar-conversion efficiencies for a theoretical, optimized full system based on the measured properties of a half-cell photoactive electrode.

Here, we propose the use of Pt and RuO_2 as state-of-the-art cathodic and anodic counter electrodes, respectively, for the purpose of calculating optimized system efficiencies based on measurements of half-cell *I-E* characteristics. The performance characteristics of these suggested counter electrode materials are shown in Table 3.1. The parameters j_0 and b are the exchange current density and Tafel slope, respectively, that fit the overpotential-current density relationship of the exemplary planar dark electrocatalysts [1]. The data in Table 3.1 were taken from previously reported electrochemical data on prepared Pt and RuO_2 electrodes. The electrodes should be prepared using the same methods (see references in Table 3.1) to avoid any convolution of electrochemical activity with differences in catalyst structuring. Additionally, any future improvements on the preparation of these or other electrodes for HER and OER should supersede the data in this table. Other reference systems can be used instead, but their equivalent electrochemical parameters should be clearly specified when calculating such optimal solar-conversion efficiencies.

Table 3.1 Performance characteristics of state-of-the-art cathodic (Pt) and anodic (RuO_2) counter electrodes.

Electrode	Electrolyte	$J_0 = \frac{I_0}{A}$ / mA cm^{-2}_{geo}	$b = \frac{2.3RT}{\alpha\, n_e F}$ /V $decade^{-1}$	Ref
Pt	Acid	1[a]	0.035[a]	26-28
Pt	Base	0.7	0.120	29
RuO_2	Acid	10^{-5}	0.035	30, 31
RuO_2	Base	10^{-5}	0.042	32

[a]Note that the kinetic parameters used here to describe the performance of Pt in acid are summarized from studies conducted with planar Pt electrodes, which are appropriate as engineering parameters that approximate the measured Tafel behavior for a planar electrode. It has been suggested that planar Pt electrodes are sufficiently active in acidic conditions such that their kinetic parameters are analogous to the calculated Nernstian diffusion overpotential assuming infinitely fast reaction kinetics, and are therefore may not be related to the true kinetics of the underlying reaction.[29, 33]. Note that for this table, the expected overpotential can be calculated using the equation $\eta = b * log\left(\frac{I}{I_o}\right)$.

The solar-conversion efficiency of the optimized half-cell is then readily calculated (Equation 5), by assuming that the series resistances are zero and using the measured photoactive electrode characteristics in conjunction with the assumed counter electrode behavior, in conjunction with the definition of a system efficiency presented in Equation (3).

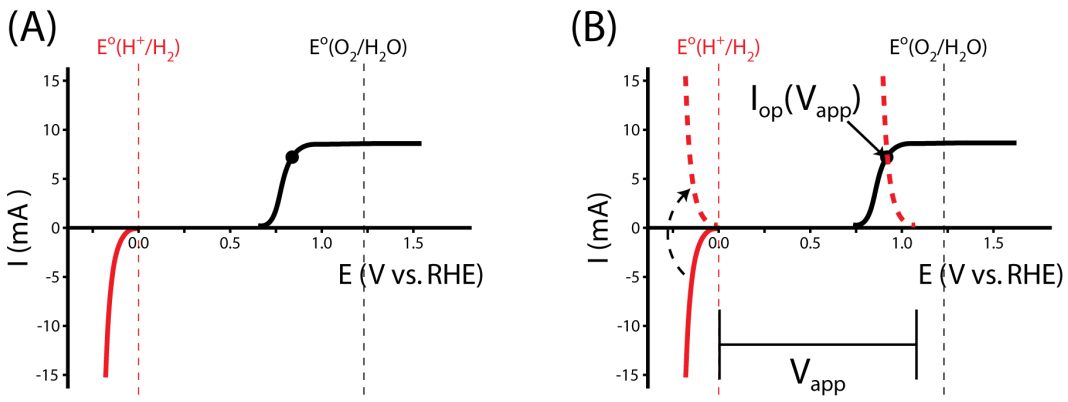

Figure 3.4. Graphical circuit analysis for a photoanode performing photo-assisted water electrolysis. (A) The characteristic three-electrode *I-E* voltammograms for a photoanode (black, positive current densities) and dark cathode (red, negative current densities). (B) A graphical circuit analysis example to determine the value for the bias-assisted (V_{app}) operating current at the maximum power point (black dot) of a photoelectrochemical system constructed from the photoactive electrodes in (A). This relationship is found by inverting the *I-E* voltammogram for the dark cathode, and shifting the resulting voltammogram by an applied potential (dashed red line) to find the operating current $I_{op}(V_{app})$ at that applied potential.

3.5.1.3 Photoelectrosynthetic Cell Efficiencies

In general, semiconductors that utilize a significant portion of the solar spectrum do not provide sufficient photovoltage, or have the correct valence/conduction band-edge alignment, to simultaneously perform the hydrogen-evolution and water-oxidation reactions when in contact with an aqueous electrolyte. For instance, to split water, semiconductors such as Si, WO_3, and Fe_2O_3 require an external bias to a counter electrode. Figure 3.4a shows a typical *I-E* characteristic of a photoanode in alkaline electrolytes, along with a Pt cathode that acts as the counter electrode and is the state-of-the-art hydrogen-evolving cathode in this hypothetical system.

The graphical circuit analysis can be used to determine the efficiency of a system that used this photoactive electrode. Figure 3.4b shows the shifted cathodic voltammogram required to determine the operating current as a function of the applied bias: $I_{op}(V_{app})$. The system has negligible operating current until sufficient bias is supplied. In this example, the $I_{op}(V_{app})$ relationship can be used to find the efficiency of this system for a given bias V_{app} from Equation (3) :

$$\eta_{opt}(V_{app}) = \frac{\boldsymbol{I_{op}}(V_{app})[C\ s^{-1}] * \Delta G[J\ C^{-1}] * \varepsilon_{elec}}{I_{op}(V_{app}) * V_{app} + P_S[W\ cm^{-2}] * A[cm^2]} \quad (20)$$

where ΔG is the Gibbs free energy supplied to water splitting, ε_{elec} is the Faradaic efficiency of the heterogeneous reaction and P_s is the power supplied by the illumination.

The properties of the counter electrode used in this analysis can be measured directly in another three-electrode measurement. Typically, η_{opt} at zero applied bias can be calculated as $\eta_{opt}(V_{app}=0)$. However, the current is negligible for this example when $V_{app}=0$, and thus there is no reason to calculate the value of η_{opt} at zero bias in this system.

3.5.1.4 Dual Photoactive Electrode System Efficiencies

The value of η_{opt} for a Z-scheme system composed of a photoanode and photocathode independently performing water oxidation and hydrogen evolution reactions, respectively, is possible with the graphical circuit analysis as well, though some additional considerations must be made for the conditions under which the "representative" *J-E* measurements are performed.[34, 35] One example of a Z-scheme is a system in which the photoanode and photocathode are arranged in a side-by-side configuration under illumination [36]. As each photoactive electrode has an independent

surface area, the P_s must be appropriately adjusted to calculate the proper efficiency. Another device architecture consists of two semiconductors in series with respect to the incident illumination, rather than in parallel such as in the side-by-side cell arrangement. Voltammograms should be measured for the second material that account for the reduced illumination intensity due to absorption in the first material. For planar materials, this attenuation can be accounted for by using an optical high-pass filter to emulate the first absorber (with a cut-off energy corresponding to the band-gap energy of the top absorber) in the measured voltammogram of the second absorber. For structured electrodes, this characteristic becomes difficult to account for, but this issue should be addressed in any report of η_{opt}.

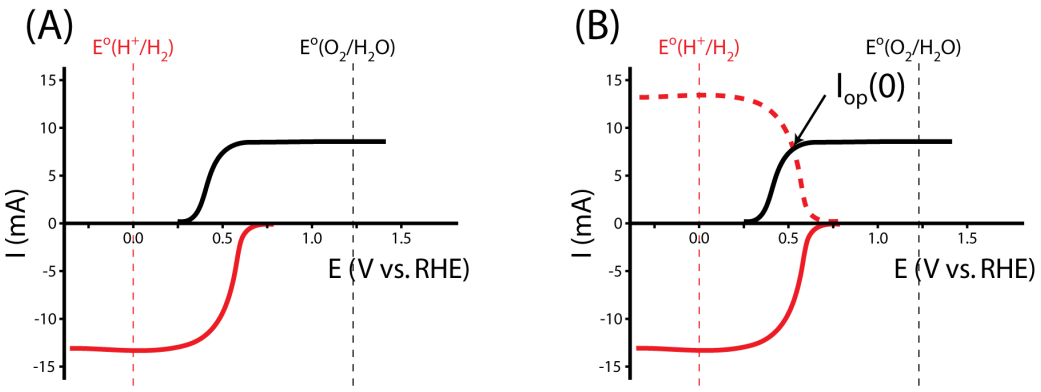

Figure 3.5. Graphical circuit analysis for a Z-scheme architecture comprised of a hypothetical photoanode and photocathode pair. (A) Characteristic three-electrode *I-E* voltammograms for the photoanode (black, positive current densities) and photocathode (red, negative current densities). (B) A graphical circuit analysis example to determine the value for the bias-free operating current $I_{op}(0)$ of a Z-scheme system constructed from the photoactive electrodes in (A).

Figure 3.5a shows the relevant *I-E* measurements for the example photocathode and photoanode materials under the same operating conditions. The intersection of the transformed photocathode voltammogram and the photoanode voltammogram in Figure 3.5b indicates the J_{op} for which η_{opt} can be calculated.

The power output at the current density $I_{op}(0)$ is given by:

$$P_{f,o} = I_{op}(0) * \Delta G \quad (21)$$

where ΔG is the difference of the thermodynamic half-cell potentials of the electrochemical reactions at the cathode and anode. The overall full photosynthetic system efficiency is then given by:

$$\eta_{FP,opt} = \frac{I_{op}(0)*\Delta G}{P_S} \quad (22)$$

For a solar-driven water-splitting system, the overall system efficiency is then given by:

$$\eta_{STH,opt} = \frac{I_{op}(0)*1.23\ V}{P_S} \quad (23)$$

Equation 23 is analogous to Equation 5 if the sole output is chemical fuel with assumed 100% faradaic efficiency for hydrogen and oxygen production. The dual-electrode scheme can, and has been, used to effect other reactions as well, including HBr and HI splitting [37, 38].

3.6 System Design Considerations

3.6.1 Relating Changes In Component Performance To Changes In Projected System Efficiency

The graphical circuit analysis is required because neither Φ_{ABPC} nor power-saved measurements are robust predictors of system efficiencies. Consider, for example, the five hypothetical photoanodes shown in Figure 3.5 as photoactive electrodes for oxygen evolution in 1 M H_2SO_4(aq). Table 3.2 presents the ratiometric power-saved figure-of-merit, as well as the value of Φ_{ABPC}, and the optimal system solar-conversion efficiency, $\eta_{opt,}$ based on the half-cell performance of each electrode.

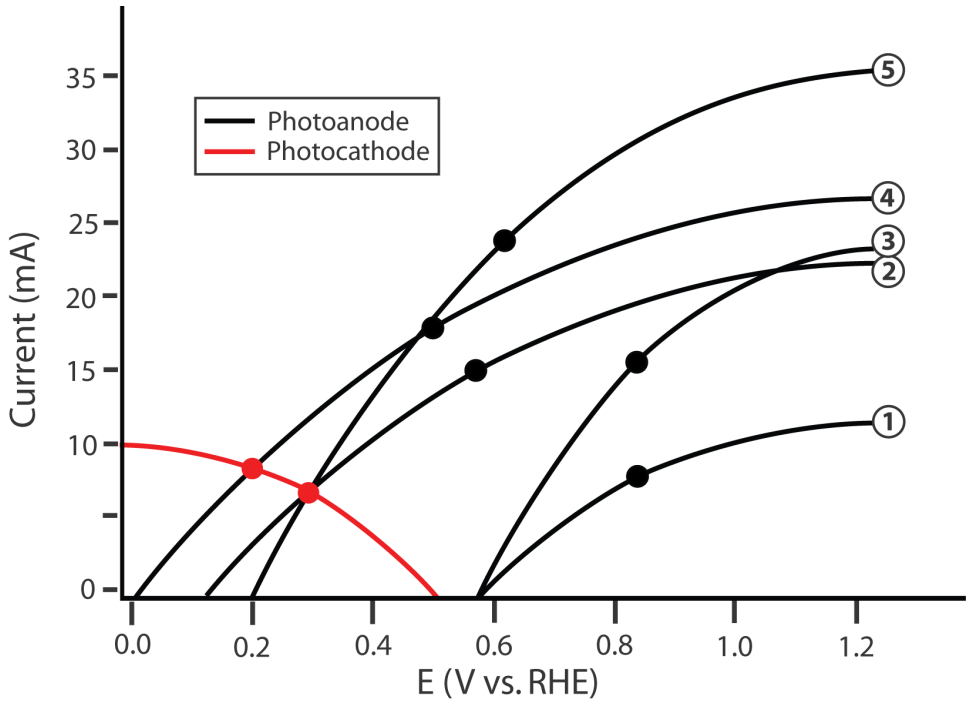

Figure 3.6. Schematic graphical circuit analysis showing five separate photoanodes (numbered on the right) and a single photocathode. The values in Table 3.2 are calculated based on this plot. The black points represent the maximum power point of each individual curve.

Electrode	V_{mp} / V	I_{mp} / mA	$\phi_{ABPC,opt}$ [a] / %	ϕ_{saved} [b] / %	$\eta_{PAE,opt}$ [a] / %	I_{op} / mA	$\eta_{STH,opt}$ / %
1	0.84	7.67	2.75	4.57	8.84	-	0.00
2	0.57	14.96	9.26	13.1	16.9	6.62	8.14
3	0.84	15.58	5.43	9.46	16.9	-	0.00
4	0.50	17.94	12.3	17.0	20.1	8.39	10.3
5	0.62	23.79	13.4	19.8	25.2	6.62	8.14

[a]Assumes an optimized Pt counter electrode with the performance metrics of Table 3.1.
[b]Compared to an optimized, state-of-the-art dark RuO_2 electrode.

Table 3.2. Half-cell performance metrics of the five photoanodes shown in figure 3.5, as well as full-cell optimal system efficiencies when each photoanode is paired either with a state-of-the-art dark counter electrode or instead with the example photocathode whose *I-E* characteristic is shown in figure 3.6.

Clearly, the model *I-E* characteristics show disparities in the efficiency and performance figures-of-merit for the various model photoanodes. However, no individual component efficiency or figure-of-merit is an adequate descriptor of the overall performance of the optimized full system. As shown in figure 3.6, photoanode 5 has the highest Φ_{ABPC} and power-saved (with respect to a state-of-the-art dark electrode) metric values of all of the photoanodes considered. A theoretical water-splitting system consisting of photoanode 3 operating at the maximum power point of the photoactive electrode, in series with an optimal Pt counter electrode and an external bias, has a maximum system efficiency of 16.7%. However, a similar system using photoanode 2 also operates with a system conversion efficiency of 16.7%. Hence, the power-saved

figures-of-merit for these two photoanodes do not indicate that the device incorporating photoanode 2 can operate with the same maximum solar-conversion efficiency as a system that instead uses photoanode 3.

A similar issue arises for the relationship between the actual system efficiencies of dual photoactive electrode systems and trends in Φ_{ABPC}, power saved measurements, or even η_{IRC} values. For example, when used in conjunction with the example photocathode to produce a whole system, the system composed of photoanode 5 operates with $\eta_{STH,opt}$ equal to that of the system comprised of photoanode 2. Moreover, using the example photocathode, neither photoanode 1 nor photoanode 3 are capable of providing the photovoltage necessary to operate in a dual-electrode full photosynthetic system with only solar power as the only source of input power. The graphical circuit analysis illustrates that although photoanode 5 yields a higher value of I_{mp} than photoanode 4, the photoanode current is not the limiting factor in this example, because due to its higher photovoltage, photoanode 4 yields a higher η_{STH} than photoanode 5 when paired with the specific photocathode used in the example of Figure 3.6. This issue demonstrates the importance of current matching when combining photoanodes and photocathodes in systems designed for photoelectrolysis.

3.6.2 Limitations of Using STH Efficiencies Relative to Using System Efficiencies

As demonstrated in Table 3.2, there are clear limitations to using η_{STH} as the sole metric for the efficiency of a photovoltaic electrosynthetic or photoelectrochemical

device. A motivating example is the case of two high-fill-factor solar cells (eg. GaAs) electrically connected in series driving electrolysis on a dark anode and a dark cathode (Figure 3.7a). In this case, the component characteristics (i.e., the *J-V* characteristics of each photovoltaic) do not change, but the values of the computed figures-of-merit may change significantly when the system is organized in different ways. For example, consider two identical photovoltaic cells that each provide 1.0 V of open-circuit voltage, 28 mA cm^{-2} of short-circuit current density, $ff = 0.86$, have optically active areas of 1 cm^2, and thus each have efficiencies of 24%. The series connection of the two photovoltaics (laid out to cover twice the area of the incident optical plane and thus receive twice the illumination as an individual cell) still has an efficiency of 24%, but produces twice the voltage and the same, matched current through the whole circuit. If an electrolysis unit that is 75% efficient at the 28 mA cm^{-2} current density is then connected with these two series-connected PV cells, the whole system has an efficiency of 18% (0.75 x 0.24), as given by Equation 3.

However, if the identical PV devices were wired individually to electrolysis units and η_{STH} was calculated by treating the whole set of components as a full system, various values would be obtained for different configurations of the identical components. Specifically, if only one PV unit was wired to an electrolysis unit and the other was unused, η_{STH} would be undefined, because η_{STH} is limited to systems in which the production of H_2 occurs spontaneously with only sunlight as the input power source, and the single PV unit does not provide sufficient voltage to perform water splitting. If the second PV was wired in series with the first and connected to the remainder of the system components, η_{STH} would then be calculated to be (28 / 2) x 1.23 = 17.4%, provided that

the electrolyzer was 75% efficient at the operating current density. If instead the electrolyzer were 60% efficient, which would require operation at a total of 1.23 V / 60% = 2.05 V, η_{STH} would again be undefined, since the total open-circuit photovoltage of 2.0 V produced by both of the PV cells connected electrically in series would be insufficient to spontaneously drive the water-splitting process and thus no electrolysis current would result.

Note that in each case, however, if additional electrical power inputs and electrical power outputs were considered, the general expression of Equation 3 for the system efficiency and Equation 4 for the solar energy-conversion efficiency would be applicable in each instance, and hence would provide for a consistent basis for comparison of the performance of these different systems.

Specifically, the system can be analyzed with the graphical circuit method by dividing the system into a tandem configuration consisting of a single PV-oxygen-evolving-photoanode and a PV-hydrogen-evolving-photocathode. Separate voltammetric measurements in a three-electrode configuration can be used for each of these two components, as shown in figure 3.7a. Figure 3.7b shows the *J-E* characteristics of each electrode in this schematic example. The potential of each electrode is defined relative to the fuel-forming reaction it performs, so the operating current for a water splitting system built from these electrodes can be evaluated from the graphical circuit analysis. Neither electrode is capable of performing the full water-splitting reaction with only a dark counter electrode, but together both electrodes are able to drive water splitting when configured in tandem. The graphical circuit analysis shown in figure 3.7c demonstrates

that an operating current can be found and the STH efficiency can be calculated from that quantity.

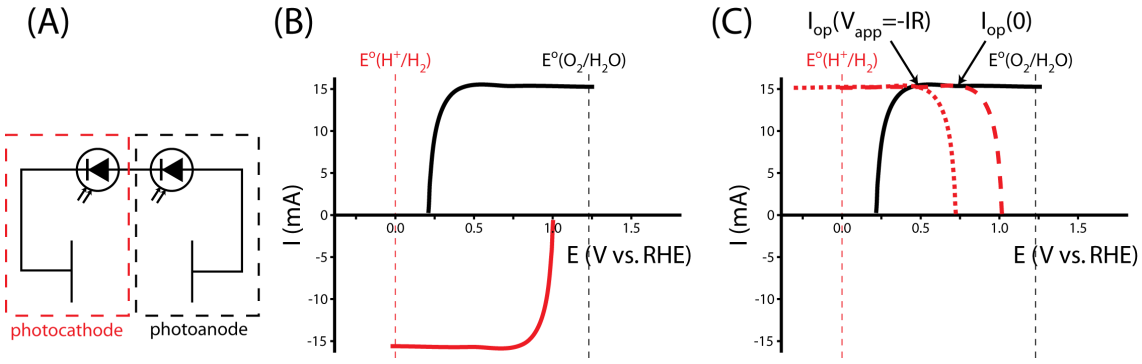

Figure 3.7. (A) The circuit diagram for a tandem photovoltaic system powering the dark electrolysis of water. (B) Schematic voltammograms for the photoanode (blue) and photocathode (red) electrodes. These voltammograms are representative of GaAs photovoltaic cells coupled in series to a hydrogen-evolving electrocatalyst (cathode) or to an oxygen-evolving electrocatalyst (anode). (C) The graphical circuit analysis of the voltammograms in (B). As each voltammogram is relatively flat near the operating current I_{op}, the addition of a resistive load to the series circuit ($I_{op}(V_{app}= -IR)$, dotted red line) results in a very similar operating current and STH efficiency as the system at short circuit with no load ($I_{op}(0)$, dashed red line), with additional electrical power being generated.

The tandem system provides a relatively large overvoltage for water splitting, which reduces the STH efficiency of the system compared to the solar-to-electricity efficiency that would be measured if the two PV units were connected in series across an optimized electrical load. Figure 3.7c shows that the voltammograms are relatively flat in the region of the operating point, due to attaining their light-limited operating current. An electrical load can be added to the series circuit, which draws excess power without

significantly affecting the operating current driving water splitting. In the graphical circuit analysis, the effect of the load drawing excess power is represented by shifting the transformed voltammogram of the photocathode to more negative potentials, effectively acting as a negative applied bias that can be utilized as electrical power. But more practically, this behavior demonstrates the necessity of load matching in solar fuels applications. A system designed from PV elements as described here would have a much higher efficiency if the architecture of the system matched the power supplied by the photocurrent-generating electrodes. A network of identical photoactive electrodes, current/voltage transformers, and electrolysis units can be assembled to minimize these overvoltages, maximizing η_{STH} without any alteration to the PEC characteristics of the photoactive electrodes [39]. It is difficult to determine the optimal system architecture from a direct STH measurement, because the PEC performance of the electrode is convoluted with the design of the experimental system. The system architecture effects are eliminated in the calculation of η_{opt} from three-electrode cyclic voltammetry measurements, thereby allowing for the absolute ceiling of efficiency to be calculated for that specific photoactive electrode or combination of electrodes. The value of η_{opt} calculated in this way is a significant metric by which to judge the technological potential of any photoactive electrode for performing solar-driven, fuel-forming reactions.

3.6.3 Systems-Level Considerations for Comparison Between Efficiencies of Different Types of Photoelectrosynthetic Cells

The systems described herein are generally part of larger processes, which may include energy needed to provide suitably pure input water streams, conditioning and pressurization of the output gas stream, and other processes involved with the storage, transportation, and utilization of the fuel[40, 41]. The overall process efficiency will be affected by many variables; for instance a 12% efficient solar-driven water-splitting system that produces H_2(g) at 1 atm pressure and thus requires a relatively inefficient 3-stage compressor to produce pressurized H_2(g) at the factory gate may be less preferred than a 10% efficient solar-driven water-splitting system that utilizes electrochemical compression and thus allows the use of a much more efficient two-stage compressor as part of the process. The key attributes of the system of interest must thus be clearly specified so that their utility in larger processes can be evaluated on a consistent basis.

A second level of complexity is introduced in assessing the efficiency of a system that produces separated fuels from a system that co-evolves the gases in a mixture in the effluent stream. To be useful in a fuel cell, for example, or in a controllable combustion-based device, the gases must be separated and thus entropy is involved as well as energy inputs. Additionally, in the specific case of solar-driven water splitting (and likely in general for any fuel production), the H_2 concentration in the O_2 (and vice versa) must never exceed the lower explosive limits at any point in the system, to be qualified as intrinsically safe and therefore to be practical and deployable (or even demonstrated at significant scale). The energy required to separate the products must therefore be included in any overall system efficiency measurement to provide a valid comparison

between the system-level efficiency of a system that produces separate, pure gas streams relative to a system that co-evolves the gases. Additionally, due to impediments to practical implementation, systems that are not intrinsically safe should be so designated, and cannot directly be compared in efficiency to systems that are intrinsically safe.

A related, third level of complexity is that in the case of solar-driven water splitting, a pressure differential along a pipeline infrastructure is required to beneficially collect the H_2 for use, and a further pressurization is required to supply, utilize, and distribute the H_2 for conversion or other end-use. The efficiency of a mechanical compressor is a strong function of the ratio of the input and output pressures of the compressed gas, whereas electrochemical compression is inherently more efficient than mechanical compression. Therefore, energy-conversion efficiencies at the systems level need to specify the output pressure of the (acceptably pure) H_2 gas stream and will need to remain functional as a system under pressure differentials that vary in both space and time.

3.7 Conclusion

The key system-level figure-of-merit for power-conversion systems is the *system efficiency,* η, obtained from the ratio of the total output power in all forms to the total input power in all forms. Use of the system efficiency provides a consistent approach for comparing the performance of various methods for producing fuels and/or electrical power. The system efficiency reduces to the *solar-to-hydrogen efficiency* (η_{STH}) for the special case of a system in which sunlight is the only input power and for which the only

useful output power is the hydrogen obtained from solar-driven water splitting; thus, η_{STH} is defined for characterizing this specific type of system.

While efficiencies are the most important measure of the performance of a full system, other single electrode and system metrics provide important characterization of electrode performance. For example, a measured efficiency value does not provide insight into the detailed behavior of individual components within the system, and therefore pathways to improvement can be obscured. This issue is particularly relevant to photoelectrochemical systems for fuel or electricity production, where dual electrodes must be independently optimized to operate in tandem within the electrochemical device. Three-electrode electrochemical measurements should be used to probe the *J-E* behavior of a specific working electrode. To compare performance among individual electrodes, a variety of figures-of-merit have been discussed, each of which has a useful role, provided that they are clearly specified and quoted in the appropriate context.

The *ideal regenerative cell efficiency* (η_{IRC}) is defined as the efficiency of a photoactive electrode component after correcting for the mass transport and uncompensated resistance overpotentials that arise because of the geometry of the electrochemical cell and used in conjunction with an ideally polarizable counterelectrode that is performing the reverse half-reaction of that performed at the photoactive electrode. This figure-of-merit can be readily reproduced between laboratories, does not require constraints regarding cell design, and is not a function of the properties of the counter electrode used in the measurement. As the name suggests, η_{IRC} is designed to yield a standardized measure of the combined photo- and catalytic performance of a photoactive

electrode, and is thus suitable for comparing performance between electrodes for fuel- and electricity-forming systems.

The *ratiometric power-saved* (ϕ_{saved}) figure-of-merit can also be used to decouple the fundamental properties of electrodes from systems engineering considerations. This figure-of-merit provides a comparison between behavior of a photoactive electrode under illumination and that of an appropriately chosen dark electrode. ϕ_{saved} yields different information depending on the dark electrode chosen for comparison, as demonstrated in Figure 3.1. If a state-of-the-art catalytic electrode for the reaction of interest is used for comparison (Table 3.1), $\phi_{saved,SOA}$ is a measure of the combined photo- and catalytic performance of a photoactive electrode. Alternatively, if a non-photoactive and oppositely and degenerately doped version of a photoactive electrode is used for comparison, $\phi_{saved,NPAC}$ is a measure of the fundamental photovoltaic performance of the photoactive electrode, because other losses in the cell (uncompensated solution resistance, mass transfer overpotential, catalytic overpotential, etc.) make identical contributions to each measurement and therefore cancel in the comparison. A judicious choice of the dark electrode must be made and specified for this calculation, as improper choices can result in arbitrarily high values of ϕ_{saved}.

A third component metric, the *applied bias photon-to-current* figure-of-merit (Φ_{ABPC}), is useful for isolating the contribution of the photovoltage of an electrode to the energy stored in the chemical products produced by the system. For systems that produce fuel from sunlight and that do not require an applied bias, Φ_{ABPC} reduces to the solar-to-fuel efficiency (such as η_{STH}).

Graphical circuit analysis methods, where three-electrode voltammograms from two different (photo)electrodes are combined on one plot, and where the crossing point of the curves is the optimal operating current of the system (which is dependent on the applied bias) are required to predict system efficiencies from individual three-electrode *I-E* measurements. This information can be used to calculate an *optimal system efficiency*, η_{opt}, which represents the maximum possible efficiency attainable when these two electrodes are combined into a system. Such a method is useful because it is often difficult to build and test a full system, but a graphical circuit analysis allows for optimal efficiencies to be estimated based on separate three-electrode measurements of individual photoactive electrodes. This method also offers the benefit of highlighting how changes within a single component electrode would affect the estimated efficiency of a full STH system, thus indicating effective utilization strategies for optimizing these components towards improving full system performance.

The various metrics described and discussed herein yield different information and all have some utility, in the proper context, for characterizing electrodes or systems for photoelectrochemical energy conversion. It is imperative that researchers choose appropriate metrics to describe the performance of electrodes and materials for such systems, and that the measurements and methods used to calculate efficiencies and figures-of-merit are properly described and denoted in full. Such an approach is critical to facilitate accurate comparisons between laboratories, and to therefore accelerate progress in the field.

TABLE 3.3:
Names and Definitions for System, Subsystem, and Component Efficiencies

System Efficiencies		
η	General expression	$\frac{P_{f,o} + P_{e,o}}{P_s + P_{e,i}}$
η_{PV}	Photovoltaic system efficiency (Solar to Electricity)	$\frac{P_{e,o}}{P_s} = \frac{I \cdot V}{P_s}$
η_{STF}	Solar-to-fuels efficiency	$\frac{P_{f,o}}{P_s} = \frac{A\,[cm^2]\,J_{sc}\,[A\,cm^{-2}] \cdot E_{f,o}[V] \cdot \varepsilon_{elec}}{P_s\,[W]}$
η_{STH}	Solar-to-hydrogen efficiency	$\frac{A\,[cm^2]\,J_{sc}\,[A\,cm^{-2}] \cdot 1.23[V] \cdot \varepsilon_{elec}}{P_s\,[W]}$
$\eta_{\text{electrolyzer}}$	Electrolyzer (Electricity-to-fuels) efficiency	$\frac{P_{f,o}}{P_{e,i}} = \frac{E_f}{V_i}$
η_{PAE}	Photoassisted electrolyzer efficiency	$\frac{P_{f,o}}{P_s + P_{e,i}}$
$\eta_{FP,opt}$	Optimal system efficiency for solar-to-fuel for a full photosynthetic cell	$\frac{I_{op}(0) \cdot \Delta G}{P_s}$
$\eta_{STH,opt}$	Optimal system efficiency for solar-to-hydrogen for a full photosynthetic cell	$\frac{I_{op}(0) \cdot 1.23\,V}{P_s}$
$\eta_{opt}(V_{app})$	System efficiency from a graphical circuit analysis	$\frac{I_{op}(V_{app})[C\,s^{-1}] \cdot \Delta G[J\,C^{-1}] \cdot \varepsilon_{elec}}{I_{op}(V_{app}) \cdot V_{app} + P_s[W\,cm^{-2}] \cdot A[cm^2]}$

Component or Half-Cell Performance Metrics

η_{IRC}	Ideal regenerative cell efficiency	$\frac{V_{mp} \cdot I_{mp}}{P_s} = \frac{I(E(A\,/A^{-})) \cdot V_{oc} \cdot ff}{P_s}$
ϕ_{saved}	Ratiometric power-saved metric	$\frac{I \cdot V_{saved}\,(I)}{P_s}$
Φ_{ABPC}	Applied-bias photon-to-current component metric	$I_{mp} \cdot \frac{(E_{f,o} - V_{ext,mp})}{P_s}$

3.8 Glossary

A	geometric surface area
$E(A/A^-)$	half-cell Nernst potential for the electrochemical reaction at the electrode referenced to the reference electrode
$E_{dark}(I)$	potential needed to drive a reaction at current I in the dark during three-electrode measurements
$E_{dark,SOA}(I)$	potential needed to drive a reaction at current I on a state-of-the-art dark electrode during three-electrode measurements
$E_{ext}(I)$	potential at the working electrode when passing current I referenced to the reference electrode
$E_{f,o}$	potential difference corresponding to the Gibbs free energy difference between the two half-reactions of the fuels being produced
$E_{light}(I)$	potential needed to drive a reaction at current I in the light during three-electrode measurements
E_{oc}	open circuit potential
ff	photovoltaic fill factor
I	current
I_{mp}	current at maximum power point
$I(E(A/A^-))$	current at the Nerstian potential for a half-reaction (corrected for solution composition)
I_0	reverse saturation current of an electrode
I_{op}	system operating current (note that I_{op} can be a function of V_{app}, $I_{op}(V_{app})$
I_{ph}	photogenerated current
I_{sc}	photovoltaic short circuit current
J	current density
$J(E(A/A^-))$	current density at the Nernstian potential for a half-reaction (corrected for solution composition)
J_{sc}	short-circuit current density
J_{fp}	current density at the formal potential of the half-reaction of interest
J_{op}	system operating current density(note that J_{op} can be a function of V_{app}, $J_{op}(V_{app})$
k	Boltzmann's constant
n	diode ideality factor
P_i	total input power
$P_{e,i}$	input electrical power
$P_{e,o}$	output power in the form of electricity
$P_{f,o}$	output power contained in the chemical fuel
P_{max}	maximium power output of a system or component
P_o	total output power
P_s	input power from solar illumination
$P_{saved}(I)$	power saved at current I
q	elementary charge on an electron

R_a	resistance associated with the anode of a system
R_c	resistance associated with the cathode of a system
R_m	membrane ohmic resistance
R_{sol}	solution ohmic resistance
T	temperature in Kelvin
V_{app}	electrical bias applied to a circuit
$V_{cat}(I)$	catalyst kinetic overpotential at current I
$V_{cat,dark}(I)$	catalyst kinetic overpotential at a dark electrode at current I
$V_{cat,light}(I)$	catalyst kinetic overpotential at a photoactive electrode
$V_{counter}(I)$	overpotential at the counter electrode at current I
$V_{dark}(I)$	external bias values needed to drive a reaction in the dark in a two-electrode system at current I
$V_{e,i}$	external electrical voltage input
V_{ext}	voltage supplied by an external source
$V_{e,o}$	output voltage of the electrical power portion of the total system output
$V_{light}(I)$	external bias values needed to drive the reaction at current I in the light in a two-electrode system
V_{mp}	voltage at maximum power point
$V_{mt}(I)$	mass-transport overpotential at current I
$V_{mt,dark}$	mass-transport overpotential at a dark electrode at current I
$V_{mt,light}$	mass-transport overpotential at a photoactive electrode at current I
V_{oc}	photovoltaic open-circuit voltage
$V_{PV}(I)$	voltage across a photoactive electrode at current I
$V_{saved}(I)$	difference between the external biases needed to drive a reaction at current I in the light and the dark on a photoactive working electrode and a related dark working electrode in a three-electrode measurement
$V_{sol}(I)$	total voltage drop across the solution resistance at current I
ΔG	Gibbs free energy per electron of the heterogeneous reaction
ε_{elec}	Faradaic efficiency
η	efficiency
$\eta_{electrolyzer}$	electrolyzer (electricity-to-fuels) system efficiency
$\eta_{FP,opt}$	full photosynthetic system efficiency calculated from graphical circuit analysis of half cell performances
η_{IRC}	ideal regenerative cell efficiency
η_{opt}	System efficiency calculated from load-line analysis of half-cell performances
η_{PAE}	photo-assisted electrolyzer system efficiency
η_{PV}	photovoltaic (solar-to-electricity) component performance metric
η_{STF}	solar-to-fuels conversion efficiency
η_{STH}	solar-to-hydrogen conversion efficiency
$\eta_{STH,opt}$	maximum solar-to-hydrogen conversion efficiency calculated from load-line analysis of half-cell performances
ϕ_{ABPC}	applied bias photon-conversion component metric

ϕ_{saved}	three-electrode power-saved performance metric
$\phi_{saved,ideal}$	three-electrode power-saved performance metric for a photoactive electrode compared to an ideally non-polarizable working electrode
$\phi_{saved,SOA}$	three-electrode power-saved performance metric for a photoactive electrode compared to the state-of-the-art (SOA) dark working electrode for the half-reaction of interest
$\phi_{saved,NPA,C}$	three-electrode power-saved performance metric for a photoactive electrode compared to an identically engineered (catalyst, substrate), but non-photoactive, working electrode (NPA,C = non-photoactive, identical catalyst)
$\phi_{saved,PA}$	three-electrode power-saved performance metric for a photoactive electrode compared to an identically engineered, but non-photoactive, working electrode without a catalyst
$\phi_{saved,poor}$	three-electrode power-saved performance metric for a photoactive electrode compared to a non-state of the art, high-overpotential working electrode

3.9 Acknowledgments

The bulk of this work appeared in *Energy and Environmental Science* in 2015 (DOI: 10.1039/c5ee00777a). I would like to thank Sonja Francis, Matt McDowell, Victoria Dix, and Shawn M. Chatman for their invaluable assistance. I would also like to particularly acknowledge Rob Coridan for his tireless efforts in improving this work.

3.10 References

1. M. G. Walter, E. L. Warren, J. R. McKone, S. W. Boettcher, Q. Mi, E. A. Santori and N. S. Lewis, *Chem. Rev.*, 2010, **110**, 6446-6473.
2. T. J. Jacobsson, V. Fjällström, M. Edoff and T. Edvinsson, *Energy Environ. Sci.*, 2014, **7**, 2056-2070.
3. A. Steinfeld, *Solar Energy*, 2005, **78**, 603-615.
4. M. A. Rosen, *Energy*, 2010, **35**, 1068-1076.
5. Z. Wang, R. R. Roberts, G. F. Naterer and K. S. Gabriel, *Int. J. Hydrogen Energy*, 2012, **37**, 16287-16301.
6. R. E. Blankenship, D. M. Tiede, J. Barber, G. W. Brudvig, G. Fleming, M. Ghirardi, M. R. Gunner, W. Junge, D. M. Kramer, A. Melis, T. A. Moore, C. C. Moser, D. G. Nocera, A. J. Nozik, D. R. Ort, W. W. Parson, R. C. Prince and R. T. Sayre, *Science*, 2011, **332**, 805-809.
7. Z. Chen, T. F. Jaramillo, T. G. Deutsch, A. Kleiman-Shwarsctein, A. J. Forman, N. Gaillard, R. Garland, K. Takanabe, C. Heske, M. Sunkara, E. W. McFarland, K. Domen, E. L. Miller, J. A. Turner and H. N. Dinh, *J. Mater. Res.*, 2010, **25**, 3-16.
8. B. A. Pinaud, J. D. Benck, L. C. Seitz, A. J. Forman, Z. Chen, T. G. Deutsch, B. D. James, K. N. Baum, G. N. Baum, S. Ardo, H. Wang, E. Miller and T. F. Jaramillo, *Energy Environ. Sci.*, 2013, **6**, 1983-2002.
9. J. R. Bolton, S. J. Strickler and J. S. Connolly, *Nature*, 1985, **316**, 495-500.
10. S. Hu, C. Xiang, S. Haussener, A. D. Berger and N. S. Lewis, *Energy Environ. Sci.*, 2013, **6**, 2984-2993.

11. A. C. Nielander, M. R. Shaner, K. M. Papadantonakis, S. A. Francis and N. S. Lewis, *Energy Environ. Sci.*, 2015, **8**, 16-25.

12. O. Khaselev, A. Bansal and J. A. Turner, *Int. J. Hydrogen Energy*, 2001, **26**, 127-132.

13. Z. Chen, H. N. Dinh and E. Miller, *Photoelectrochemical Water Splitting - Standards, Experimental Methods, and Protocols*, Springer, 2013.

14. G. J. Conibeer and B. S. Richards, *Int. J. Hydrogen Energy*, 2007, **32**, 2703-2711.

15. M. S. Wrighton, A. B. Ellis, P. T. Wolczanski, D. L. Morse, H. B. Abrahamson and D. S. Ginley, *J. Am. Chem. Soc.*, 1976, **98**, 2774-2779.

16. B. Parkinson, *Acc. Chem. Res.*, 1984, **17**, 431-437.

17. J. K. Dohrmann and N.-S. Schaaf, *J. Phys. Chem.*, 1992, **96**, 4558-4563.

18. A. J. Bard, R. Memming and B. Miller, *Pure Appl. Chem.*, 1991, **63**, 569-596.

19. H. Dotan, N. Mathews, T. Hisatomi, M. Grätzel and A. Rothschild, *J. Phys. Chem. Lett.*, 2014, **5**, 3330-3334.

20. M. X. Tan, P. E. Laibinis, S. T. Nguyen, J. M. Kesselman, C. E. Stanton and N. S. Lewis, in *Progress in Inorganic Chemistry*, ed. K. D. Karlin, John Wiley & Sons, Inc., 1994, pp. 21-144.

21. A. Heller, *Acc. Chem. Res.*, 1981, **14**, 154-162.

22. A. Heller and R. G. Vadimsky, *Phys. Rev. Lett.*, 1981, **46**, 1153-1156.

23. H. Gerischer, *Electrochimica Acta*, 1990, **35**, 1677-1699.

24. S. Hu, M. R. Shaner, J. A. Beardslee, M. Lichterman, B. S. Brunschwig and N. S. Lewis, *Science*, 2014, **344**, 1005-1009.

25. K. Sun, F. H. Saadi, M. F. Lichterman, W. G. Hale, H.-P. Wang, X. Zhou, N. T. Plymale, S. T. Omelchenko, J.-H. He, K. M. Papadantonakis, B. S. Brunschwig and N. S. Lewis, *Proc. Natl. Acad. Sci. U. S. A.*, 2015, **112**, 3612-3617.

26. J. O. M. Bockris, B. Dandapani, D. Cocke and J. Ghoroghchian, *Int. J. Hydrogen Energy*, 1985, **10**, 179-201.

27. N. M. Marković, B. N. Grgur and P. N. Ross, *J. Phys. Chem. B*, 1997, **101**, 5405-5413.

28. H. Kita, S. Ye and Y. Gao, *J. Electroanal. Chem.*, 1992, **334**, 351-357.

29. W. Sheng, H. A. Gasteiger and Y. Shao-Horn, *J. Electrochem. Soc.*, 2010, **157**, B1529-B1536.

30. G. Lodi, E. Sivieri, A. D. Battisti and S. Trasatti, *J. Appl. Electrochem.*, 1978, **8**, 135-143.

31. S. Haussener, C. Xiang, J. M. Spurgeon, S. Ardo, N. S. Lewis and A. Z. Weber, *Energy Environ. Sci.*, 2012, **5**, 9922-9935.

32. M. E. G. Lyons and S. Floquet, *Phys. Chem. Chem. Phys.*, 2011, **13**, 5314-5335.

33. K. C. Neyerlin, W. Gu, J. Jorne and H. A. Gasteiger, *J. Electrochem. Soc.*, 2007, **154**, B631-B635.

34. M. Grätzel, *Nature*, 2001, **414**, 338-344.

35. Y. Tachibana, L. Vayssieres and J. R. Durrant, *Nat. Photonics*, 2012, **6**, 511-518.

36. S. Licht, in *Semiconductor Electrodes and Photoelectrochemistry*, Wiley, 2002.

37. C. Levy-Clement, A. Heller, W. A. Bonner and B. A. Parkinson, *J. Electrochem. Soc.*, 1982, **129**, 1701-1705.

38. L. Fornarini, A. J. Nozik and B. A. Parkinson, *J. Phys. Chem.*, 1984, **88**, 3238-3243.

39. T. L. Gibson and N. A. Kelly, *Int. J. Hydrogen Energy*, 2008, **33**, 5931-5940.

40. P. Zhai, S. Haussener, J. Ager, R. Sathre, K. Walczak, J. Greenblatt and T. McKone, *Energy Environ. Sci.*, 2013, **6**, 2380-2389.

41. J. A. Herron, J. Kim, A. A. Upadhye, G. W. Huber and C. T. Maravelias, *Energy Environ. Sci.*, 2014, **8**, 126-157.